International Journal of Innovative
Computing, Information and Control
Volume **9**, Number **6**, June **2013**

 ISSN 1349-4198
pp. **2619–2634**

A NOVEL ACTIVE FILTER FOR UNBALANCED 3-PHASE 4-WIRE POWER SYSTEM BASED ON LINEAR ADAPTIVE NOTCH FILTER AND FUZZY ADAPTIVE HYSTERESIS CONTROLLER

Xiaochu Qiu[1,2], Peng Shi[3,4], Jian Xiao[1] and Jun Wang[2]

[1]School of Electrical Engineering
Southwest Jiaotong University
No. 111, North Section 1, 2nd Ring Road, Chengdu 610031, P. R. China
xh_qiusir@mail.xhu.edu.cn; Jxiaomail@tom.com

[2]School of Electrical and Information Engineering
Xihua University
No. 999, Jinzhou Road, Chengdu 610039, P. R. China
jiayu@mail.sc.cninfo.net

[3]School of Engineering and Science
Victoria University
Melbourne, 8001 VIC, Australia

[4]School of Electrical and Electronic Engineering
The University of Adelaide
Adelaide, SA 5005, Australia
peng.shi@vu.edu.au

Received March 2012; revised July 2012

Abstract. *In this paper, a novel active power filter (APF) for 3-phase 4-wire power (3P4W) system under unbalanced non-linear load and various non-ideal mains voltage test cases is presented. The determination of current references for APF with 4-leg inverter is based on linear adaptive notch filter and instantaneous symmetrical components algorithm. The fuzzy adaptive hysteresis band current control strategy is developed, where the band is modulated with the system parameters to maintain the modulation frequency nearly constant. Simulation experiment results are presented to verify the effectiveness and the viability of the proposed APF.*

Keywords: 3-phase 4-wire power system, 4-leg shunt active power filter, Linear adaptive notch filter, Instantaneous symmetrical component, Fuzzy adaptive hysteresis band current control

1. **Introduction.** Nowadays, 3-phase 4-wire distribution power system has been widely used in residential and office buildings, manufacturing facilities, schools, etc., to supply low level voltage. The typical loads connected to the 3-phase 4-wire power system may be balanced 3-phase non-linear loads such as motor drivers, silicon controlled rectifiers, large un-interruptible power supplies or single phase non-linear loads such as switch-mode power supplies in computer equipment, inverter air conditioners and other power electronic related facilities. Most of these loads have a nonlinear input or unbalanced characteristic, which may cause two problems of high input current harmonics and excessive neutral current [1]. The existence of current harmonics in power systems increases losses in the lines, decreases the power factor and causes timing errors in sensitive electronic equipment. The harmonic currents produced by balanced 3-phase non-linear loads are positive-sequence harmonics and negative-sequence harmonics. However, harmonic currents produced by single phase non-linear loads which are connected phase to neutral in a 3-phase 4-wire

system are third order zero-sequence harmonics. These triplen harmonic currents unlike positive and negative-sequence harmonic currents do not cancel but add up arithmetically at the neutral bus. This can result in neutral current that can reach magnitudes as high as 1.73 times the phase current [2]. Since the size of the neutral conductor is usually less than the size of the phase conductor, excessive neutral current may cause overheat, which may potentially damage the neutral conductor and distribution transformer while affecting the safety of the consumers.

Two fundamental approaches for improving power quality are passive filter and active filter. Passive filters are widely used to eliminate harmonics in power system for its simplicity and low cost. However, passive filters have several drawbacks such as large size, tuning and risk of resonance problems. At present, the 4-leg active filters have proven to be very effective to solve problems of current harmonics, reactive power, unbalanced load current and excessive neutral current simultaneously in 3-phase 4-wire system, and can be a much better solution than conventional passive filters.

The detection of harmonics and compensation strategies are very important components of APF. Instantaneous reactive power (IRP) theory was introduced by Akagi et al. at the beginning of the 1980s [3]. It has been used very successfully to design and control of the active power filter (APF) for 3-phase 3-wire system and was extended by Aredes et al. [4], for applications in 3-phase 4-wire systems. The IRP theory was widely applied to calculate the compensating currents assuming ideal mains voltages. However, mains voltage may be unbalanced and/or distorted in industrial systems. Therefore, the 4-leg APF using the p-q theory does not provide good performance [2]. For improving the APF performance under non-ideal mains voltage conditions, various improved methods based on IRP have been proposed [5-11] while good results have been achieved. However, IRP methods for harmonic detection in the 3P4W systems need phase-locked-loop (PLL), low-pass filter and the complex coordinate transformation. In this paper, a novel harmonics detection algorithm under unbalanced-distorted mains voltage case in 3P4W system based on linear adaptive notch filter without PLL and low-pass filter is proposed; the amplitude and phase of fundamental positive sequence component of load current are accurately extracted. An ideal notch filter (NF) is a linear filter whose frequency response is characterized by a unit gain at all frequencies except at a particular frequency called the notch frequency at which its gain is zero. Such an ideal filter is not feasible and a realistic NF is characterized by its bandwidth. The original version of the adaptive notch filter (ANF) in a lattice-based discrete-time form was first proposed by Regalia [12]. Regalia's algorithm was later adopted for continuous-time by Bodson and Douglas [13] and finally a modified version of the original algorithm was proposed in [14]. Since then, ANF is widely applied to power system as a signal analysis, individual signal follow and harmonics detection [15-17]. Recently, it has become popular signal analysis algorithm for no DFT frequency leakage, no strict demands of time window and no wavelet basis functions selection.

There are various compensation strategies proposed for active power filter; hysteresis current control strategy has the highest rate among other current control strategies such as sinusoidal PWM. Because it is very simple and easy to implement, hysteresis current control strategy is widely used in active power filter for its high precision, good stability and dynamic performance, but has several known disadvantages such as uncontrollable high switching frequency and induced important switching losses. Some interesting improved versions of this technique are presented in literature [18-21]. Fuzzy logic is an alternative approach to handle this type of problem, which has become more popular during past four decades due to its advantages of robustness against parameter variation, popularity, customization, etc., [22-28]. Use of fuzzy logic for hysteresis current control is not a new issue; rather various authors have introduced some innovative methodologies

using this tool [29]. According to the literature [30] shows the relation of the hysteresis band; a fuzzy adaptive hysteresis controller (FAHC) is proposed in this paper. Because the hysteresis band of the hysteresis current controller can adapt as variety of the current deviation and supply voltage, the switching frequency and switch frequency range can be reduced effectively.

This paper presents a novel linear adaptive notch filter and fuzzy hysteresis controller based active power filter for 3P4W system, the harmonic current compensation and the elimination of the neutral current are effectively achieved under unbalanced non-linear load and various non-ideal mains voltage test cases. The system considered in this paper is shown in Figure 1. Section 2 of this paper provides the fundamentals of 3P4W APF. In Section 3, linear adaptive notch filter algorithm, instantaneous symmetrical component algorithm and fuzzy adaptive hysteresis band current control strategy are considered. Finally, simulation results verify the feasibility and validity of the proposed 3P4W APF.

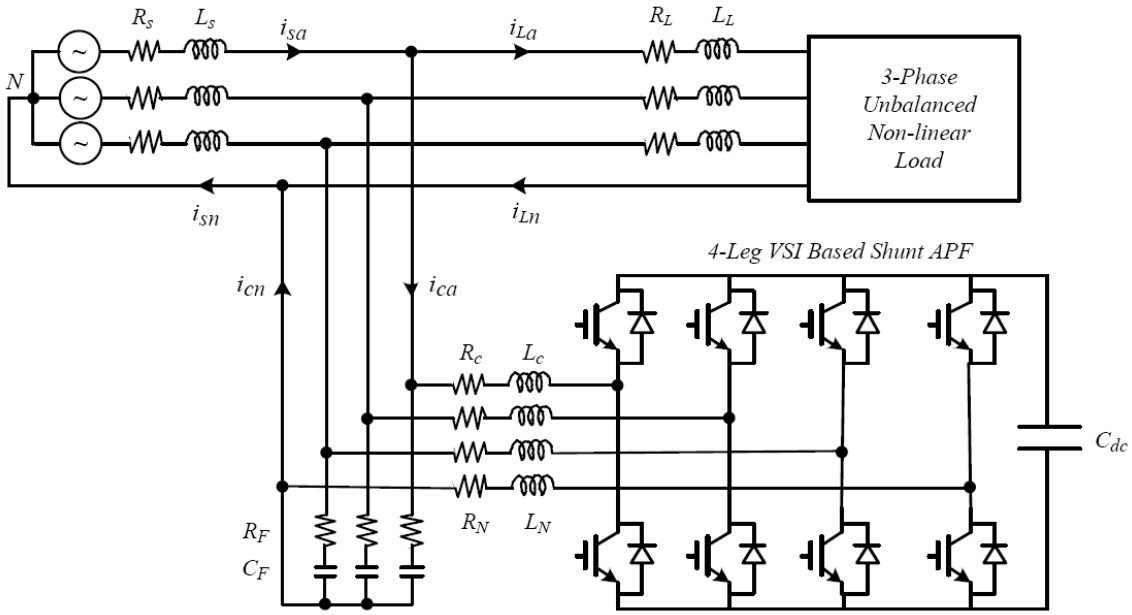

FIGURE 1. Power circuit of the 4-leg shunt APF

2. **Shunt Active Power Filter.** The main objective of the 4-leg APF is to compensate harmonics, reactive power, neutral current and unbalancing of non-linear loads locally. In 3-phase 4-wire systems, two kinds of VSI topologies such as 4-leg inverter and 3-leg inverter (split capacitor) are used. The 4-leg inverter uses 1-leg specially to compensate zero sequence (neutral) current. Figure 1 shows the basic compensation principle of the shunt APF. A shunt APF is designed to be connected in parallel with the load, to detect its harmonic current and to inject into the system a compensating current, identical with the load harmonic current. Therefore, the current drawn from the power system at the coupling point of the filter will result in sinusoidal.

3. **Description of the Proposed Method.** The active power filter proposed for 3-phase 4-wire power system under unbalanced non-linear loads and non-ideal mains voltage cases consists of linear adaptive notch filter algorithm, instantaneous symmetrical components algorithm and fuzzy hysteresis current controller strategy. The harmonic detection algorithm proposed employs a linear adaptive notch filter to extract asymmetrical

fundamental component for each phase respectively. The fundamental positive sequence component in the asymmetrical fundamental component can be obtained with instantaneous symmetrical component algorithm.

3.1. **linear adaptive notch filter algorithm.** The input signal of linear adaptive notch filter is given as follows:

$$\begin{aligned} i(t) &= I\sin(\omega t+\varphi) \\ &= I\cos\varphi\cdot\sin\omega t + I\sin\varphi\cdot\cos\omega t \end{aligned} \tag{1}$$

where ω denotes angle frequency.

According to [31], the statue variables are selected as Equation (2).

$$\mathbf{x}(t) = \begin{bmatrix} x_1(t) \\ x_2(t) \end{bmatrix} = \begin{bmatrix} I\cos\varphi \\ I\sin\varphi \end{bmatrix} \tag{2}$$

Therefore, the estimate $\hat{i}(t)$ can be expressed as:

$$\hat{i}(t) = x_1(t)\cdot\sin\omega t + x_2(t)\cdot\cos\omega t \tag{3}$$

The deviation between $i(t)$ and $\hat{i}(t)$ is given as:

$$e(t) = i(t) - \hat{i}(t) \tag{4}$$

According to least squares, the cost function can be defined as:

$$J(\mathbf{x}) = 0.5e^2(t) = 0.5(i(t)-\hat{i}(t))^2 \tag{5}$$

Using the gradient descent method, therefore

$$\dot{\mathbf{x}} = -\boldsymbol{\mu}\frac{\partial J(x)}{\partial x} \tag{6}$$

where $\boldsymbol{\mu}$ is a coefficient matrix to adjust $x(t)$ to the optimal convergence speed and stability.

Assume $\mu_1, \mu_2 > 0$, $\boldsymbol{\mu}$ can be defined as:

$$\boldsymbol{\mu} = \begin{bmatrix} \mu_1 & 0 \\ 0 & \mu_2 \end{bmatrix} \tag{7}$$

Thus, the following linear dynamic system can be obtained:

$$\dot{\mathbf{x}} = \mathbf{A}\cdot\mathbf{x} + \mathbf{B}\cdot i(t) \tag{8}$$

where

$$\begin{aligned} \dot{\mathbf{x}} &= \begin{bmatrix} \dot{x}_1(t) & \dot{x}_2(t) \end{bmatrix}^T, \quad \mathbf{x} = \begin{bmatrix} x_1(t) & x_2(t) \end{bmatrix}^T, \\ \mathbf{A} &= \begin{bmatrix} -\mu_1\sin^2\omega t & -\mu_1\sin\omega t\cdot\cos\omega t \\ -\mu_2\sin\omega t\cdot\cos\omega t & -\mu_1\cos^2\omega t \end{bmatrix}, \\ \mathbf{B} &= \begin{bmatrix} \mu_1\sin\omega t \\ \mu_2\cos\omega t \end{bmatrix} \end{aligned}$$

Define the rotating coordinate transformation:

$$\mathbf{y}(t) = \begin{bmatrix} y_1(t) \\ y_2(t) \end{bmatrix} = \begin{bmatrix} \sin\omega t & \cos\omega t \\ \cos\omega t & -\sin\omega t \end{bmatrix}\cdot\begin{bmatrix} x_1(t) \\ x_2(t) \end{bmatrix} \tag{9}$$

So, the estimate $\hat{i}(t)$ can also be expressed as:

$$\hat{i}(t) = y_1(t) = x_1(t)\sin\omega t + x_2(t)\cos\omega t \tag{10}$$

Substituting Equation (9) into Equation (8), then

$$\begin{bmatrix} \dot{y}_1(t) \\ \dot{y}_2(t) \end{bmatrix} = \begin{bmatrix} -\mu_1 \sin^2 \omega t - \mu_2 \cos^2 \omega t & \omega \\ -\omega & 0 \end{bmatrix} \cdot \begin{bmatrix} y_1(t) \\ y_2(t) \end{bmatrix} + \begin{bmatrix} \mu_1 \sin^2 \omega t + \mu_2 \cos^2 \omega t \\ (\mu_1 - \mu_2) \sin \omega t \cdot \cos \omega t \end{bmatrix} \tag{11}$$

If $\mu_1 = \mu_2 = \mu$, $\omega = \eta$, 2-D linear filter algorithm is given as:

$$\begin{bmatrix} \dot{y}_1(t) \\ \dot{y}_2(t) \end{bmatrix} = \begin{bmatrix} -\mu & \eta \\ -\eta & 0 \end{bmatrix} \cdot \begin{bmatrix} y_1(t) \\ y_2(t) \end{bmatrix} + \begin{bmatrix} \mu \\ 0 \end{bmatrix} \cdot i(t) \tag{12}$$

where $\mathbf{y}(t) = \begin{bmatrix} y_1(t) & y_2(t) \end{bmatrix}^T$ is state variable, μ is the speed parameter of the filter to adjust the filter bandwidth and transient convergence rate, η is the center frequency parameter of the notch filter. $y_1(t)$ is output of the filter, which represents the fundamental component of the input signals, ω is the angular frequency; $y_2(t)$ is the same as $y_1(t)$ in frequency of the sinusoidal signal, but phase orthogonal each other.

Set $y_1(0) = 0$, $y_2(0) = 0$, the filter transfer function $H(s)$ is given as:

$$H(s) = \frac{\mu s}{s^2 + \mu s + \eta^2} \tag{13}$$

Substituting $s = j\omega$ into Equation (13), then:

$$H(j\omega) = \frac{j\omega\mu}{(j\omega)^2 + j\omega\mu + \eta^2} \tag{14}$$

So, the amplitude frequency characteristics of the linear adaptive notch filter is given as:

$$|H(j\omega)| = \frac{\omega\mu}{\sqrt{(\eta^2 - \omega^2)^2 + (\omega\mu)^2}} \tag{15}$$

and the phase frequency characteristics of the linear adaptive notch filter is given as:

$$\arg[H(j\omega)] = \frac{\pi}{2} - \arctan \frac{\omega\mu}{\eta^2 - \omega^2} \tag{16}$$

In the case of $\eta = \omega$, the amplitude frequency characteristics and the phase frequency characteristics of the linear adaptive notch filter are given as:

$$|H(j\omega)| = \frac{\omega\mu}{\sqrt{(\eta^2 - \omega^2)^2 + (\omega\mu)^2}} = 1 \tag{17}$$

$$\arg[H(j\omega)] = \frac{\pi}{2} - \arctan \frac{\omega\mu}{\eta^2 - \omega^2} = 0 \tag{18}$$

Therefore, while the signal frequency is equal to η, the filter will accurately track the signal amplitude and phase. As the signal frequency changes, the filter amplitude-frequency characteristic and phase-frequency characteristic curve is shown in Figure 2. As long as the parameters μ and η are selected reasonably, the filter will have a good frequency selectivity and no phase shift, accurately track the input signal frequency components specified in the amplitude and phase. The linear adaptive notch filter block diagram for the APF is shown in Figure 3.

3.2. **Instantaneous symmetrical components algorithm.** With proposed method, three linear adaptive notch filters are employed to extract 3-phase asymmetrical fundamental components respectively. The fundamental positive sequence component in the asymmetrical fundamental component can be obtained with symmetrical component algorithm. As the traditional symmetrical component method is actually to use the current value of the phase advance rather than the instantaneous value, the error may occur in the

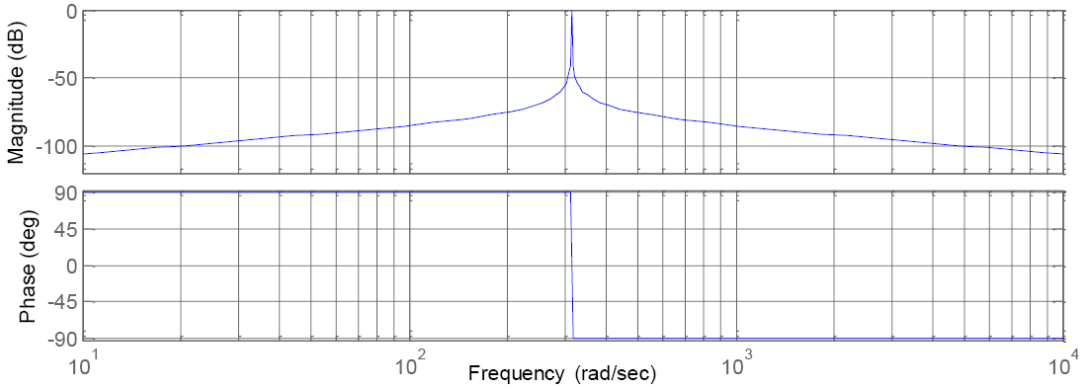

FIGURE 2. Bode plots of filter ($\mu = 0.05$, $\eta = 314$)

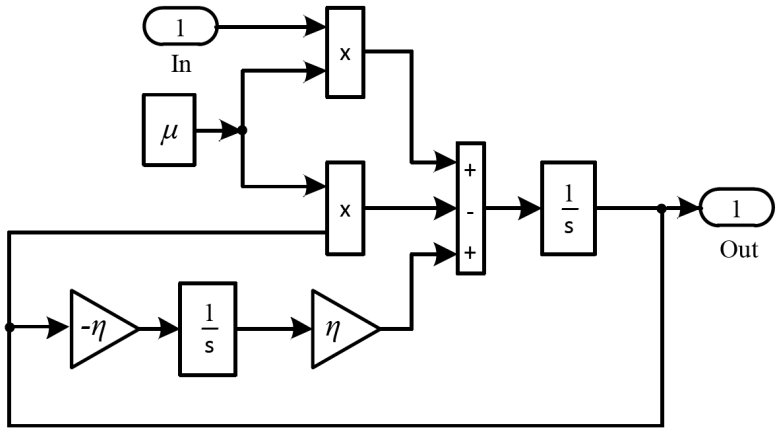

FIGURE 3. The linear adaptive notch filter block diagram

engineering applications. Therefore, a method based on the instantaneous symmetrical components is employed to extract the fundamental positive sequence component.

Assuming asymmetric three phase instantaneous current:

$$\begin{bmatrix} i_a(t) \\ i_b(t) \\ i_c(t) \end{bmatrix} = \begin{bmatrix} I_{am}\sin(\omega t + \varphi_a) \\ I_{bm}\sin(\omega t + \varphi_b) \\ I_{cm}\sin(\omega t + \varphi_c) \end{bmatrix} \tag{19}$$

where $i_a(t)$, $i_b(t)$, $i_c(t)$ denote three phase current instantaneous value respectively; I_{am}, I_{bm}, I_{cm} denote the three phase current amplitude respectively; φ_a, φ_b, φ_c denote the initial phase respectively.

Set the rotation phasor as $\dot{I}_a$, $\dot{I}_b$, $\dot{I}_c$ corresponding to three-phase current $i_a(t)$, $i_b(t)$, $i_c(t)$ respectively.

$$\begin{bmatrix} \dot{I}_a \\ \dot{I}_b \\ \dot{I}_c \end{bmatrix} = \begin{bmatrix} I_{am}\cos(\omega t + \varphi_a) + jI_{am}\sin(\omega t + \varphi_a) \\ I_{bm}\cos(\omega t + \varphi_b) + jI_{bm}\sin(\omega t + \varphi_b) \\ I_{cm}\cos(\omega t + \varphi_c) + jI_{cm}\sin(\omega t + \varphi_c) \end{bmatrix} \tag{20}$$

Because of the imaginary part of the phasor $\dot{I}_a$, $\dot{I}_b$, $\dot{I}_c$ is the instantaneous current value, as long as the real part of the phaser can be determined, the phasers can be calculated. According to the literature [32], an improved trigonometric decomposition method is used to calculate the rotating phasor.

Let phase 'A' instantaneous current value can be expressed as:

$$\begin{aligned} i_a(t) &= I_{am}\sin[\omega(t-\Delta t+\Delta t)+\varphi_a] \\ &= I_{am}\sin[\omega(t-\Delta t)+\varphi_a]\cdot\cos\omega\Delta t \\ &\quad +I_{am}\cos[\omega(t-\Delta t)+\varphi_a]\cdot\sin\omega\Delta t \end{aligned} \tag{21}$$

that is

$$\begin{aligned} i_a(t) &= i_a(t-\Delta t)\cdot\cos\omega\Delta t \\ &\quad +I_{am}\cos[\omega(t-\Delta t)+\varphi_a]\cdot\sin\omega\Delta t \end{aligned} \tag{22}$$

so

$$I_{am}\cos[\omega(t-\Delta t)+\varphi_a] = \frac{i_a(t)-i_a(t-\Delta t)\cdot\cos\omega\Delta t}{\sin\omega\Delta t} \tag{23}$$

and because

$$\begin{aligned} I_{am}\cos(\omega t+\varphi_a) &= I_{am}\cos[\omega(t-\Delta t+\Delta t)+\varphi_a] \\ &= I_{am}\cos[\omega(t-\Delta t)+\varphi_a]\cdot\cos\omega\Delta t \\ &\quad +I_{am}\sin[\omega(t-\Delta t)+\varphi_a]\cdot\sin\omega\Delta t \end{aligned} \tag{24}$$

so,

$$I_{am}\cos(\omega t+\varphi_a) = \frac{i_a(t)\cdot\cos\omega\Delta t - i_a(t-\Delta t)}{\sin\omega\Delta t} \tag{25}$$

Similarly available

$$I_{bm}\cos(\omega t+\varphi_b) = \frac{i_b(t)\cdot\cos\omega\Delta t - i_b(t-\Delta t)}{\sin\omega\Delta t} \tag{26}$$

$$I_{cm}\cos(\omega t+\varphi_c) = \frac{i_c(t)\cdot\cos\omega\Delta t - i_c(t-\Delta t)}{\sin\omega\Delta t} \tag{27}$$

Substituting Equations (25)-(27) into (20), the instantaneous rotation phasor is received, the positive sequence component of the asymmetrical three-phase current is:

$$\begin{bmatrix} i_{ap}(t) \\ i_{bp}(t) \\ i_{cp}(t) \end{bmatrix} = I_m\left\{\frac{1}{3}\begin{bmatrix} 1 & a & a^2 \\ a^2 & 1 & a \\ a & a^2 & 1 \end{bmatrix}\cdot\begin{bmatrix} \dot{I}_a \\ \dot{I}_b \\ \dot{I}_c \end{bmatrix}\right\} \tag{28}$$

where $Im\{\}$ denotes the imaginary part of complex computing requirements; $a = e^{j2\pi/3}$, $a^2 = e^{-j2\pi/3}$, $1+a+a^2 = 0$.

While the sampling time is determined, $\cos\omega\Delta t$ and $\sin\omega\Delta t$ in Equation (28) are constant, no trigonometric function numeration is required.

3.3. **Fuzzy adaptive hysteresis band current control strategy.** The conventional hysteresis control is very simple and easy to implement, but has several known disadvantages such as uncontrollable high switching frequency and induced important switching losses for its fixed hysteresis band. To improve the drawback of the conventional hysteresis control, an adaptive fuzzy hysteresis band current control technique can be programmed as a function of the active filter and supply parameters to minimize the influence of current distortions on modulated waveform. The band can be modulated at different points of fundamental frequency of the cycle to control the PWM switching pattern of the inverter.

The hysteresis band (HB) is given by [30]:

$$HB = \frac{0.125V_{dc}}{f_cL}\left[1-\frac{4L^2}{V_{dc}^2}\left(\frac{V_{sa}}{L}+\frac{di_{ca}^*}{dt}\right)\right] \tag{29}$$

where f_c is the switch frequency, V_{dc} is the DC voltage, i_{ca}^* is the source reference current and $\frac{di_{ca}^*}{dt}$ represents its slope.

Equation (29) shows that adaptive hysteresis band current control needs a precise knowledge of the APF parameters (L and V_{dc}), the switch frequency will change with changes of supply voltage and current bias differential while the hysteresis band is fixed. In order to reduce switching frequency and maintain its for constant, hysteresis band must be changed with the change of the supply voltage and the differential of reference current. As the changes of the DC voltage of the inverter is a relatively small, the approximate fixed-frequency can be achieved as long as the hysteresis band changes with the supply voltage and the differential of the reference current. While the sampling time interval is very small, the error reference current is available to approximate the deviation of the reference current. Therefore, a fuzzy controller including two input variables (error current Δi and supply voltage v_s) and output variable (hysteresis band HB) can be obtained. The block diagram of the fuzzy adaptive hysteresis band current control is shown in Figure 4. Figure 5 shows the membership functions of the input and the output variables. Each input variables is transformed into linguistic size with five fuzzy subsets, PL, PM, EZ, NL and NM. For the output variable HB, PVS is positive very small, and PVL is positive very large. The resulting rule is presented in Table 1.

4. **Simulation Results.** The proposed system shown in Figure 1 is simulated using Matlab/Simulink software under four mains voltage cases, including ideal mains voltage,

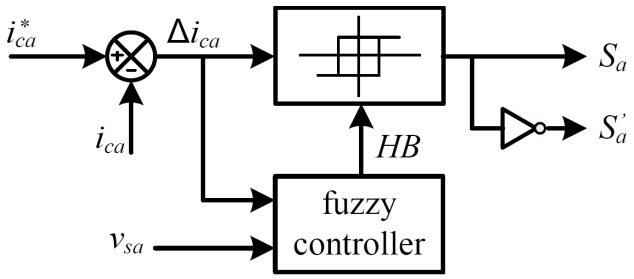

FIGURE 4. Simplified model for fuzzy adaptive hysteresis band current control

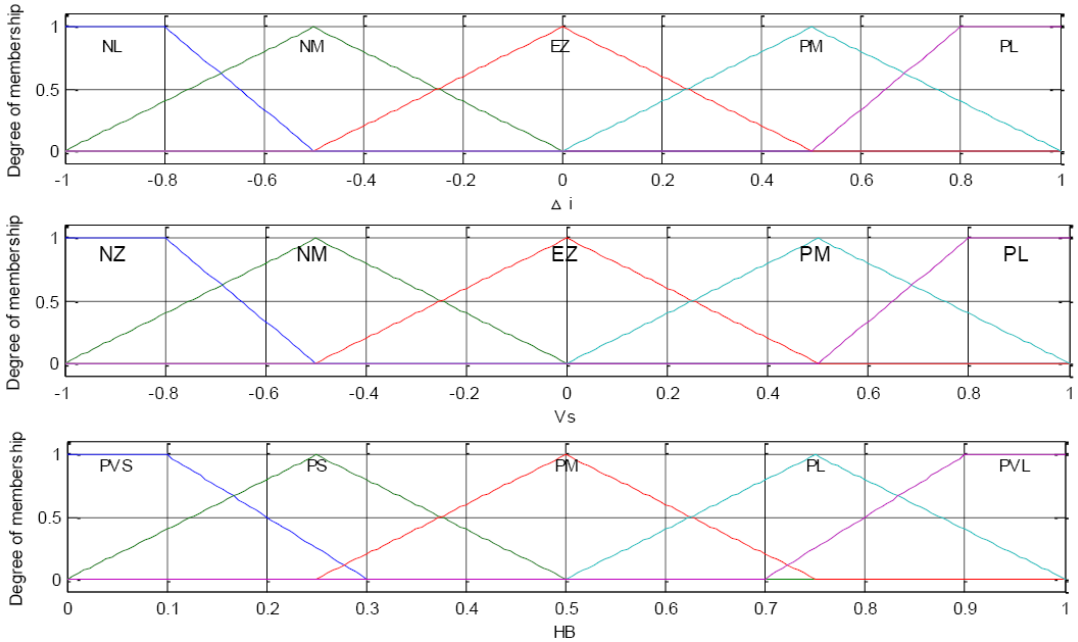

FIGURE 5. Membership functions for input variables Δi, v_s and output variable HB

TABLE 1. Rule base for the fuzzy model

voltage	current error				
	NZ	NM	EZ	PM	PL
NZ	PVS	PS	PM	PS	PVS
NM	PS	PM	PL	PM	PS
EZ	PM	PL	PVL	PL	PM
PM	PS	PM	PL	PM	PS
PL	PVS	PS	PM	PS	PVS

unbalanced mains voltage, balanced-distorted mains voltage and unbalanced-distorted mains voltage cases. The purpose of the designed case studies is to show the validity and performance of the proposed APF, even if the mains voltages are highly distorted and unbalanced. The parameters of 3P4W APF system are shown as Table 2. The three phase unbalanced non-linear load is composed by a three phase diode rectifier feeding an R-L load and two single phase R-L loads. The comprehensive simulation results are discussed below.

TABLE 2. System parameters used in simulation

Parameter	Value
Source	
Voltage (V_{sabc})	220Vrms/phase-neutral
Frequency (f)	50Hz
Impedance (R_S, L_S)	10mΩ, 50μH
4-Leg shunt APF	
DC-link voltage (V_{dc})	800V
DC capacitor (C_{dc})	1500μF
Switching frequency (f_s)	40kHz/average
AC side filter (R_C, L_C), (R_F, C_F)	(0.1Ω, 1mH), (2Ω, 20μF)
Load	
3-Phase Load	12Ω, 20mH
1-Phase diode rectifier	15Ω, 1mH, 470μF
Filter	
Frequency parameter (η)	314rad/s
Speed parameter (μ)	1.8 ($t < 0.01s$), 0.5 ($t > 0.01s$)

4.1. **Ideal mains voltage case.** Figure 6(b) shows the harmonic current filtering and load current balancing simulation results with proposed method for the 4-leg APF under ideal mains voltages. The neutral current is successfully canceled with proposed control methods as shown in Figure 6(d). The reactive power compensation simulation results with proposed method is shown in Figure 6(e). Compensated source currents are in phase with 3-phase mains voltages. Detailed summary of load currents, source currents and their total harmonic distortion (THD) levels are shown in Table 3. The proposed method is feasible under ideal mains voltages case.

4.2. **Unbalanced mains voltage case.** For this case, the unbalanced 3-phase mains voltages are shown in Equation (30). The power system has not zero-sequence voltage

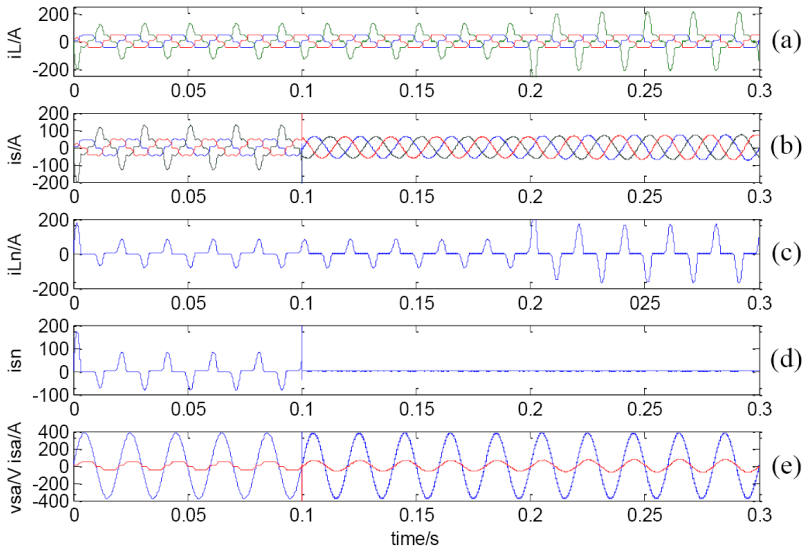

FIGURE 6. Load current (a), source current (b), load neutral current (c), source neutral current (d) and reactive power compensation (e) under ideal mains voltage case

TABLE 3. Summary of load current, source current and their THD under ideal main voltage case

A, B, C, N	load current		source current	
	$t < 0.2$s	$t > 0.2$s	0.1s $< t <$ 0.2s	$t > 0.2$s
THD (%)				
A phase	20.08	20.08	2.03	3.12
B phase	40.83	63.67	1.90	1.90
C phase	20.07	20.07	0.85	3.12
Neutral	78.39	78.34	–	–
RMS (A)				
A phase	47.21	47.19	63.83	73.57
B phase	131.04	216.21	63.25	73.57
C phase	47.19	47.20	62.73	72.53
Neutral	84.68	169.04	0.38	0.43

component.

$$\begin{cases} v_{ab} = 380\sin(\omega t) + 38\sin(\omega t) \\ v_{bc} = 380\sin(\omega t - 120^\circ) + 38\sin(\omega t + 120^\circ) \\ v_{ca} = 380\sin(\omega t + 120^\circ) + 38\sin(\omega t - 120^\circ) \end{cases} \tag{30}$$

Harmonic current suppression and load current balancing simulation results with proposed method for the 4-leg APF under unbalanced mains voltages are shown in Figure 7(b). Since the harmonic detection method proposed has nothing to do with mains voltage, negative-sequence component of mains voltage with the proposed method has no effect, after compensation 3-phase source currents are balanced and sinusoidal as shown in Figure 7(d). The neutral current elimination and reactive power compensation is successfully done with proposed control methods as shown in Figure 7(e). Detailed summary of load currents, source currents and their THD levels are shown in Table 4. The unbalanced mains voltage in a 3-phase 4-wire power system will not affect the 4-leg APF performance with proposed algorithm.

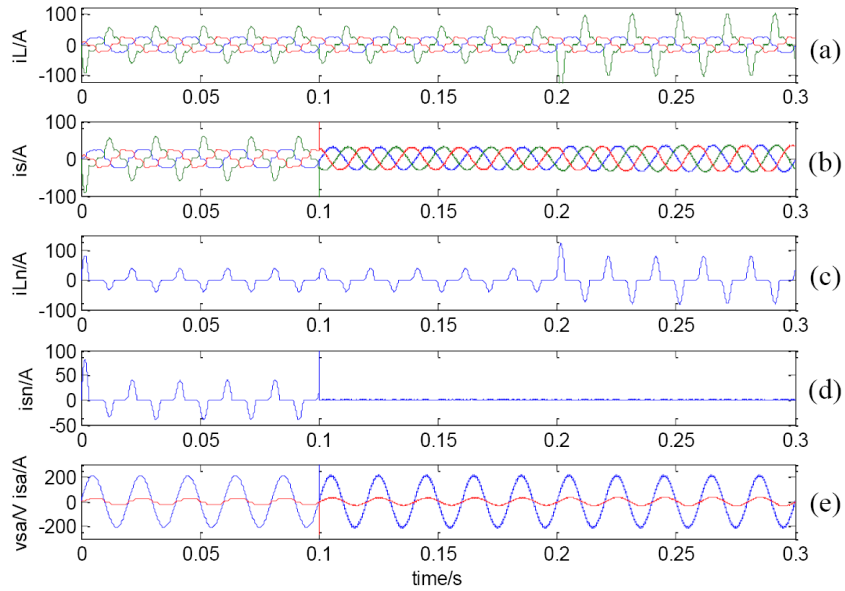

FIGURE 7. Load current (a), source current (b), load neutral current (c), source neutral current (d) and reactive power compensation (e) under unbalanced mains voltage case

TABLE 4. Summary of load current, source current and their THD under unbalanced main voltage case

A, B, C, N	load current		source current	
	$t < 0.2$s	$t > 0.2$s	0.1s $< t <$ 0.2s	$t > 0.2$s
THD (%)				
A phase	17.22	17.22	1.94	3.00
B phase	39.34	51.55	1.14	1.27
C phase	23.11	23.11	1.91	2.92
Neutral	78.46	78.4	–	–
RMS (A)				
A phase	23.84	23.84	31.65	36.77
B phase	61.11	101.24	31.12	37.23
C phase	23.85	23.85	29.94	35.65
Neutral	40.27	80.40	0.44	0.48

4.3. **Balanced-distorted mains voltage case.** When 3-phase mains voltages are balanced-distorted, mains voltages contain harmonic voltage components except fundamental component. 3-Phase balanced-distorted mains voltage is expressed as Equation (31)

$$\begin{cases} v_{ab} = 380\sin\omega t + 4.56\sin 3\omega t + 22.8\sin(5\omega t - 120^\circ) \\ \qquad +5.7\sin 7\omega t + 3.8\sin(11\omega t - 120^\circ) \\ v_{bc} = 380\sin(\omega t - 120^\circ) + 4.56\sin 3\omega t + 22.8\sin 5\omega t \\ \qquad +5.7\sin(7\omega t - 120^\circ) + 3.8\sin 11\omega t \\ v_{ca} = 380\sin(\omega t + 120^\circ) + 4.56\sin 3\omega t + 22.8\sin(5\omega t + 120^\circ) \\ \qquad +5.7\sin(7\omega t + 120^\circ) + 3.8\sin(11\omega t + 120^\circ) \end{cases} \tag{31}$$

Figure 8(b) shows that the harmonic current filtering and load current balancing simulation results with proposed method for the 4-leg APF under balanced distorted mains voltages. While the load current THD level is 39.26% before 0.2s, 49.45% after 0.2s in

phase B. 3-Phase source currents are balanced and sinusoidal after compensation with the proposed method and THD level of source current after compensation is 2.34% during $0.1 < t < 0.2$s and 2.19% after 0.2s in phase B. Figure 8(d) and Figure 8(e) show the neutral current elimination and reactive power compensation performance with three control methods for the 4-leg APF, respectively. At the same time, the 4-leg APF compensates reactive current of the load and improves power factor and eliminates zero-sequence current components. Detailed summary of load currents, source currents and their THD levels are shown in Table 5. There is a significant reduction in harmonic distortion level with the proposed technique. The balanced distorted mains voltage in a 3-phase 4-wire power system will not affect the 4-leg APF performance by using the proposed method.

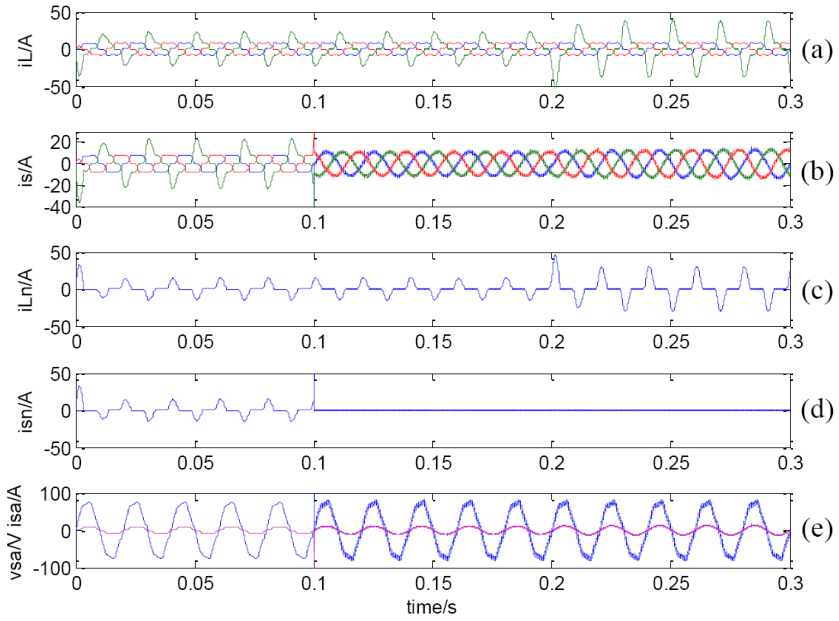

FIGURE 8. Load current (a), source current (b), load neutral current (c), source neutral current (d) and reactive power compensation (e) under balanced-distorted mains voltage case

TABLE 5. Summary of load currents, source currents and their THD levels under balanced-distorted mains voltage case

A, B, C, N	load current		source current	
	$t < 0.2$s	$t > 0.2$s	0.1s $< t <$ 0.2s	$t > 0.2$s
THD (%)				
A phase	20.01	20.01	2.75	3.23
B phase	39.26	49.45	2.34	2.19
C phase	20.98	20.98	2.69	3.12
Neutral	70.81	70.74	–	–
RMS (A)				
A phase	8.19	8.19	11.64	13.93
B phase	22.87	37.54	11.62	14.01
C phase	8.19	8.19	11.49	13.59
Neutral	14.70	29.37	0.63	0.59

4.4. **Unbalanced-distorted mains voltage case.** When 3-phase mains voltages are unbalanced and distorted, mains voltage contains negative-sequence component and harmonic voltage components. For this case, the unbalanced 3-phase mains voltages are shown Equation (32). The mains voltage waveform is shown in Figure 9.

$$\begin{cases} v_{ab} = 380\sin\omega t + 38\sin\omega t + 4.56\sin 3\omega t \\ \quad +22.8\sin(5\omega t - 120^\circ) + 5.7\sin 7\omega t + 3.8\sin(11\omega t - 120^\circ) \\ v_{bc} = 380\sin(\omega t - 120^\circ) + 38\sin(\omega t + 120^\circ) + 4.56\sin 3\omega t \\ \quad +22.8\sin 5\omega t + 5.7\sin(7\omega t - 120^\circ) + 3.8\sin 11\omega t \\ v_{ca} = 380\sin(\omega t + 120^\circ) + 38\sin(\omega t - 120^\circ) + 4.56\sin 3\omega t \\ \quad +22.8\sin(5\omega t + 120^\circ) + 5.7\sin(7\omega t + 120^\circ) \\ \quad +3.8\sin(11\omega t + 120^\circ) \end{cases} \tag{32}$$

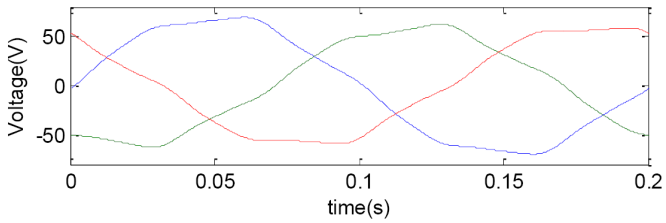

FIGURE 9. The unbalanced-distorted mains voltage waveform

Figure 10(b) shows the harmonic current filtering and load current balancing simulation results with proposed method for the 4-leg APF under unbalanced distorted mains voltages. While the load current THD level is 33.95% before $0.2s$, 43.52% after $0.2s$ in phase B. After compensation the source currents become sinusoidal and balanced with the proposed method and THD level of source current after compensation is 3.25% during $0.1 < t < 0.2s$ and 2.75% after $0.2s$ in phase B. The neutral current elimination and reactive power compensation are successfully done with proposed methods as shown in Figure 10(d) and Figure 10(e). Detailed summary of load currents, source currents and their THD levels are shown in Table 6. The unsymmetrical distorted voltage system is the most severe condition. However, good results can be obtained by the proposed theory.

TABLE 6. Summary of load currents, source currents and their THD levels under unbalanced-distorted mains voltage case

A, B, C, N	load current		source current	
	$t < 0.2$s	$t > 0.2$s	$0.1\text{s} < t < 0.2$s	$t > 0.2$s
THD (%)				
A phase	17.54	17.54	3.08	3.16
B phase	33.95	43.52	3.25	2.75
C phase	24.15	24.15	3.43	3.51
Neutral	64.47	64.41	–	–
RMS (A)				
A phase	6.96	6.96	9.49	11.46
B phase	16.54	27.15	9.65	11.56
C phase	6.96	6.96	9.31	11.08
Neutral	10.69	21.36	0.68	0.65

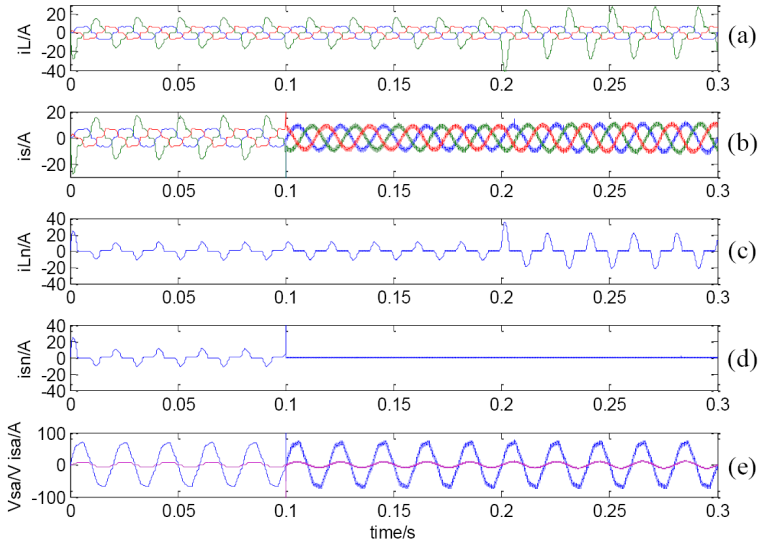

FIGURE 10. Load current (a), source current (b), load neutral current (c), source neutral current (d) and reactive power compensation (e) under unbalanced-distorted mains voltage case

4.5. **Switching performance of the inverter.** Figure 11 shows the switching frequency and its change range of the inverter simulation results with conventional hysteresis control, adaptive variable hysteresis band control and proposed control methods. As the hysteresis band of the hysteresis current controller can adapt variety of the current deviation and supply voltage, the switching frequency and switch frequency change range have been reduced effectively with the control method of the proposed. Detailed summary of the switching frequency and its change range with three control methods are shown in Table 7. In current tracking precision improvement and switch frequency reducing, good results can be obtained by the proposed control method.

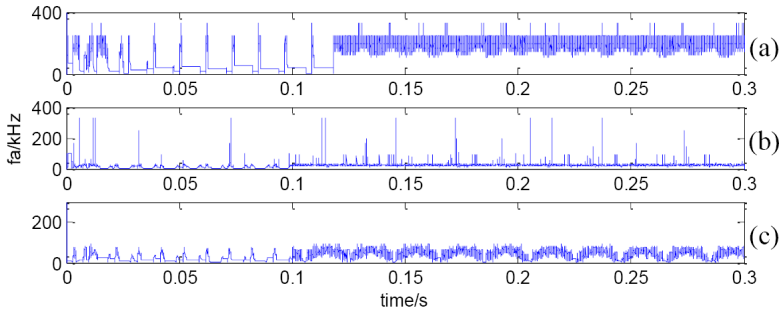

FIGURE 11. Switching frequency with conventional hysteresis band (a), adaptive variable hysteresis band (b) and proposed hysteresis band (c) control methods

5. **Conclusion.** In this paper, a linear adaptive notch filter and instantaneous symmetrical components based algorithm and fuzzy adaptive hysteresis band current control strategy are proposed. A three-phase four-wire active power filter system is studied. The performance of the 3P4W APF system is analyzed. There are no PLL, LPF and reference-frame transformation requirement with the proposed harmonic detection algorithm. The fuzzy adaptive hysteresis control strategy significantly reduces the number of switching and the variation range of switching, compared with a conventional hysteresis control.

TABLE 7. Summary of the switching frequency and its change range with three control methods

	conventional hysteresis		adaptive hysteresis		proposed hysteresis	
	$t < 0.1$s	$t > 0.1$s	$t < 0.1$s	$t > 0.1$s	$t < 0.1$s	$t > 0.1$s
THD (%)	20.08	2.01	20.08	5.48	20.08	0.03
freq. Max. (kHz)	–	250	–	330	–	80
range of freq. (kHz)	–	10-250	–	12-330	–	10-80

The APF is able to suppress current harmonics, to compensate reactive power, to balance load current and to eliminate excessive neutral current for 3-phase 4-wire power system under unbalanced non-linear loads and non-ideal mains voltage cases. Since the proposed harmonic detection algorithm and current control strategy are independent of the system parameters, the performance of the APF has a strong robustness to the variation of the system parameters. The simulation results validated the performance of the proposed APF.

Acknowledgement. This work was partially supported by National Natural Science Foundation of China (51177137, 61134001 and 61174058), Sichuan Provincial Key Discipline of Power Electronics and Electric Driver (No. SZD0503-09-0), the National Key Basic Research Program, China (2012CB215202) and the 111 Project (B12018).

REFERENCES

[1] H. Jou, K. Wu, J. Wu et al., A three-phase four-wire power filter comprising a three-phase three-wire active power filter and a zigzag transformer, *IEEE Trans. on Power Electronics*, vol.23, no.1, pp.252-259, 2008.

[2] M. Ucar and E. Ozdemir, Control of a 3-phase 4-leg active power filter under non-ideal mains voltage condition, *Electric Power Systems Research*, vol.78, no.1, pp.58-73, 2008.

[3] H. Akag, Y. Kanazawa and A. Nabae, Instantaneous reactive power compensators comprising switching devices without energy storage elements, *IEEE Trans. Industry Applications*, vol.20, no.3, pp.625-630, 1984.

[4] M. Aredes, J. Hafner and K. Heumann, Three-phase four-wire shunt active filter control strategies, *IEEE Trans. on Power Electronics*, vol.12, no.2, pp.311-318, 1997.

[5] S. Huang, J. Wu and H. Jou, A study of three-phase active power filters under non-ideal mains voltages, *Electric Power Systems Research*, vol.49, no.2, pp.125-137, 1999.

[6] C. Chen and Y. Hsu, A novel approach to the design of a shunt active filter for an unbalanced three-phase four-wire system under nonsinusoidal conditions, *IEEE Trans. Power Delivery*, vol.15, no.4, pp.1258-1264, 2000.

[7] M. Haque, T. Ise and S. ve Hosseini, A novel control strategy for active filters usable in harmonic polluted and/or imbalanced utility voltage case of 3-phase 4-wire distribution systems, *Proc. of the 9th International Conference on Harmonics and Quality of Power*, Orlando, Florida, pp.239-244, 2000.

[8] B. Lin and Y. Lee, Three-phase power quality compensator under the unbalanced sources and non-linear loads, *IEEE Trans. on Industrial Electronics*, vol.51, no.5, pp.1009-1017, 2004.

[9] G. Chang and C. Yeh, Optimisation-based strategy for shunt active power filter control under non-ideal supply voltages, *Electric Power Applications, IEE Proceedings*, vol.152, no.2, pp.182-190, 2005.

[10] H. Kim, F. Blaabjerg, B. Bak-Jensen et al., Instantaneous power compensation in three-phase systems by using *p-q-r* theory, *IEEE Trans. on Power Electronics*, vol.17, no.5, pp.701-710, 2002.

[11] Y. Komatsu and T. Kawabata, A control method for the active power filter in unsymmetrical voltage systems, *Int. J. Electron*, vol.86, no.10, pp.1249-1260, 1999.

[12] P. Regalia, An improved lattice-based IIR notch filter, *IEEE Trans. Signal Process*, vol.39, no.9, pp.2124-2128, 1991.

[13] M. Bodson and S. Douglas, Adaptive algorithms for the rejection of sinusoidal disturbances with unknown frequency, *Automatic*, vol.33, no.12, pp.2213-2221, 1997.
[14] L. Hsu, R. Oaega and G. Damm, A globally convergent frequency estimator, *IEEE Trans. Automatic Control*, vol.44, no.4, pp.698-713, 1999.
[15] M. Karimi-Ghartemani and A. K. Ziarani, Periodic orbit analysis of two dynamical systems for electrical engineering applications, *Journal of Engineering Mathematical*, vol.45, no.2, pp.135-154, 2003.
[16] M. Karimi-Ghartemani and A. K. Ziarani, Performance characterization of a nonlinear system as both an adaptive notch filter and a phase-locked loop, *International Journal of Adaptive Control Signal Process*, vol.18, no.1, pp.23-53, 2004.
[17] A. Ziarani and A. Konrad, A method of extraction of nonstationary sinusoids, *Signal Process*, vol.84, no.8, pp.1323-1346, 2004.
[18] S. Buso and L. Malesani, Comparison of current control techniques for active filter applications, *IEEE Trans. on Industrial Electronics*, vol.45, no.5, pp.722-729, 1998.
[19] S. Buso, S. Fasolo, L. Malesani et al., A dead beat adaptive hysteresis current control, *IEEE Trans. Ind. Appl.*, vol.36, no.4, pp.1174-1180, 2000.
[20] Y. Mei, G. Ding, H. Qing et al., A novel DSP based current controller with fuzzy variable-band hysteresis for active power filters, *IEEE/PES Transmission and Distribution Conference and Exhibition*, Dalian, China, pp.1-5, 2005.
[21] L. Jun and W. Zhi, Study and simulation of a novel hysteresis current control strategy, *The 2nd International Conference on Intelligent Computation Technology and Automation*, Shenyang, China, pp.306-309, 2009.
[22] J. Zhang, P. Shi and Y. Xia, Fuzzy delay compensation control for T-S fuzzy systems over network, *IEEE Trans. on Systems, Man and Cybernetics, Part B: Cybernetics*, 2012.
[23] Q. Zhou, P. Shi, J. Lu and S. Xu, Adaptive output feedback fuzzy tracking control for a class of nonlinear systems, *IEEE Trans. on Fuzzy Systems*, vol.19, no.5, pp.972-982, 2011.
[24] L. Wu, X. Su, P. Shi and J. Qiu, Model approximation for discrete-time state-delay systems in the T-S fuzzy framework, *IEEE Trans. on Fuzzy Systems*, vol.19, no.2, pp.366-378, 2011.
[25] L. Wu, X. Su, P. Shi and J. Qiu, A new approach to stability analysis and stabilization of discrete-time T-S fuzzy time-varying delay systems, *IEEE Trans. on Systems, Man and Cybernetics, Part B: Cybernetics*, vol.41, no.1, pp.273-286, 2011.
[26] J. Zhang, P. Shi and Y. Xia, Robust adaptive sliding mode control for fuzzy systems with mismatched uncertainties, *IEEE Trans. on Fuzzy Systems*, vol.18, no.4, pp.700-711, 2010.
[27] S. K. Nguang, P. Shi and S. Ding, Fault detection for uncertain fuzzy systems: An LMI approach, *IEEE Trans. on Fuzzy Systems*, vol.15, no.6, pp.1251-1262, 2007.
[28] N. Belhaouchet, L. Rahmani and S. Begag, A novel adaptive HBCC technique for three-phase shunt APF, *Electric Power Systems Research*, vol.79, no.7, pp.1097-1104, 2009.
[29] F. Mekri, M. Machmoum, N. A. Ahmed et al., A fuzzy hysteresis voltage and current control of an unified power quality conditioner, *Industrial Electronics, the 34th Annual Conference of IEEE*, Orlando, Florida, pp.2684-2689, 2008.
[30] M. Kale and E. Ozdemir, An adaptive hysteresis band current controller for shunt active power filter, *Electric Power Systems Research*, vol.73, no.2, pp.113-119, 2005.
[31] X. Qiu, J. Xiao and C. Wu, A novel harmonic current detection method for three-phase four-wire system based on linear filter, *Power System Protection and Control*, vol.39, no.9, pp.44-51,58, 2011.
[32] Y. Feng, C. Jie and W. Yu, An improved method of instantaneous symmetrical components and its detection for positive and negative sequence current, *Proc. of the CSEE*, vol.28, no.1, pp.52-58, 2008.